Available online at www.sciencedirect.com
SCIENCE DIRECT®
Journal of Solid State Chemistry 179 (2006) 2199–2205
JOURNAL OF SOLID STATE CHEMISTRY
www.elsevier.com/locate/jssc

Stable cubic spinels in the Zn–Mn–O system in air

J. Blasco*, J. García

Instituto de Ciencia de Materiales de Aragón, CSIC-Universidad de Zaragoza, Departamento de Física de la Materia Condensada, Pedro Cerbuna 12, 50009 Zaragoza, Spain

Received 16 February 2006; received in revised form 11 April 2006; accepted 16 April 2006
Available online 3 May 2006

Abstract

A part of the Zn–Mn–O phase diagram has been studied by using soft synthetic conditions and highly reactive precursors. This procedure allowed us to find and to isolate new single phases in the Zn-rich region. The new compounds are cubic spinels with a nominal composition $Mn_{3-x}Zn_xO_4$ with $x = 1.6$ and 1.7. These spinels decompose upon heating giving rise to tetragonal distorted spinels. This survey is focused on the low-temperature region ($T \leqslant 700\,^{\circ}C$) completing previous reports on the Zn–Mn–O phase diagram.

We also report the magnetic properties of the new cubic spinels. These samples behave as paramagnets obeying a Curie–Weiss law in a broad temperature range. The effective paramagnetic moment agrees with the nominal mixture of Mn^{3+} and Mn^{4+} ions. However, randomness and competitive interactions give rise to the formation of spin-glass phases at very low temperature.

PACS: 61.10.Nz; 81.30.Dz; 75.50.Pp; 75.50.Lk; 75.50.Tt

Keywords: Spinel; Phase diagram; Transparent semiconductors; Spin-glass; Magnetic semiconductors

1. Introduction

Doped ZnO has been the subject of an intense research owing to its remarkable applications in various fields of optical and electronic devices [1,2]. Among these studies, it is clear that some Mn-doped ZnO compounds exhibit a ferromagnetic component at room temperature whose origin is now subject of controversy [3–6]. In the course of our research about the existence of a ferromagnetic ground state in substituted ZnO, we realized that ferromagnetism was only obtained for samples with minor impurities supporting an extrinsic origin for such a behavior [7]. However, the use of low sintering temperature is needed to obtain the ferromagnetic impurity since high-temperature treatments always lead to non-magnetic compounds. In the case of Mn-doped ZnO, we also detected the presence of a secondary phase showing a cubic structure. This phase, identified as $ZnMnO_3$, was also observed by other researchers [8,9].

$ZnMnO_3$ was identified in a pioneering work studying the reactivity between ZnO and MnO_2 [10]. It was obtained from solid state reaction with an excess of ZnO which was removed by boiling in acetic acid [10]. The X-ray pattern of this sample was indexed in the frame of an unidentified cubic structure. However, we suspected that this cubic phase was in fact a spinel because the allowed reflections clearly agree with the $Fd\bar{3}m$ space group. Later on, other researchers were successful in preparing $ZnMnO_3$ by using high pressure methods [11]. This compound showed a hexagonal cell isostructural to the Ilmenite. These facts make us realize that the Zn–Mn–O system was not fully studied, in particular the presence of metastable phases prepared by soft methods.

The phase diagram of the Zn–Mn–O system in air was reported in the past [12] for samples prepared using the conventional ceramic method. The X-ray analysis at room temperature for $Mn_{3-x}Zn_xO_4$ ($1 \leqslant x \leqslant 2$) samples revealed the existence of tetragonally distorted spinel ($x \sim 1$), a mixture of two distorted spinels ($x \leqslant 1.5$) and a mixture of distorted spinel and ZnO ($x \geqslant 1.5$). Cubic spinels are only observed at high temperatures and for instance, the

*Corresponding author. Fax: +34 97 676 24 19.
E-mail address: jbc@unizar.es (J. Blasco).

0022-4596/$ - see front matter © 2006 Elsevier Inc. All rights reserved.
doi:10.1016/j.jssc.2006.04.026

$ZnMn_2O_4$ transforms into a cubic spinel at around 1100 °C [12]. The Zn–Mn–O system is rather reactive at high temperature (~800–900 °C), so quenching is necessary to freeze the high-temperature configuration as performed in Ref. [12]. However, sometimes the reaction kinetic is so fast that quenching could not freeze the equilibrium configuration. Besides equilibration at low temperature is so slow that very long times are required to achieve thermodynamic equilibrium. One way to overcome this handicap is the use of highly reactive precursors which react into products very fast at moderate temperatures.

The aim of the present work is to complete our knowledge of the Zn–Mn–O system at low temperature by using starting material in nano-size scale. In order to do it, we have synthesized nominal $Mn_{3-x}Zn_xO_4$ samples ($1 \leqslant x \leqslant 2$) following a sol–gel method that permits to form crystal compounds at relative low temperature [13]. This procedure allowed us to find single phases of cubic spinels which cannot be prepared by conventional solid state reaction or needs much longer sintering times. We have also studied the structural and magnetic properties of these new phases establishing a phase diagram that completes previous surveys.

2. Experimental section

Nominal $Mn_{3-x}Zn_xO_4$ ($x = 1$, 1.1, 1.3, 1.5, 1.55, 1.6, 1.7, 1.75, 1.9 and 2.0) samples were synthesized by using the citrate route. Stoichiometric amounts of ZnO and $MnCO_3$, were dissolved in nitric acid solution. Then, citric acid and ethylene–glycol were added (4 g and 2 mL/g of precursor, respectively) and light-yellow solutions were obtained. They were heated up to gel formation. The gel was fired at 210 °C overnight. The resulting brown resin was calcined in air at 400 °C for 6 h. Then, the powder was pressed into pellets and heated at selected temperatures (450°, 550°, 600°, 700° and 800°). The sintering times ranges between 16 and 136 h while the cooling rate varies from 300 °C h^{-1} up to quenching in water or air.

All samples were characterized by means of X-ray diffraction by using a D-MaxB Rigaku system. We have used Cu $K\alpha$ radiation and the patterns were measured between 15° and 80°. In order to perform profile analysis, step-scanned patterns were collected for single-phase compounds between 15° and 135° in steps of 0.03° and with a counting time of 5 s per step. Structural refinements were carried out by using the Rietveld method and the Fullprof program [14].

Magnetization measurements were carried out between 5 and 300 K in a commercial Quantum Design superconducting quantum interference device (SQUID) magnetometer. The AC magnetic susceptibility was measured in the absence of an external DC magnetic field by using an alternating field of 4 Oe and frequencies ranging between 1 and 100 Hz. DC magnetization was also determined using an external magnetic field of 1 kOe in two ways: zero-field cooled (ZFC) and field cooled (FC) conditions.

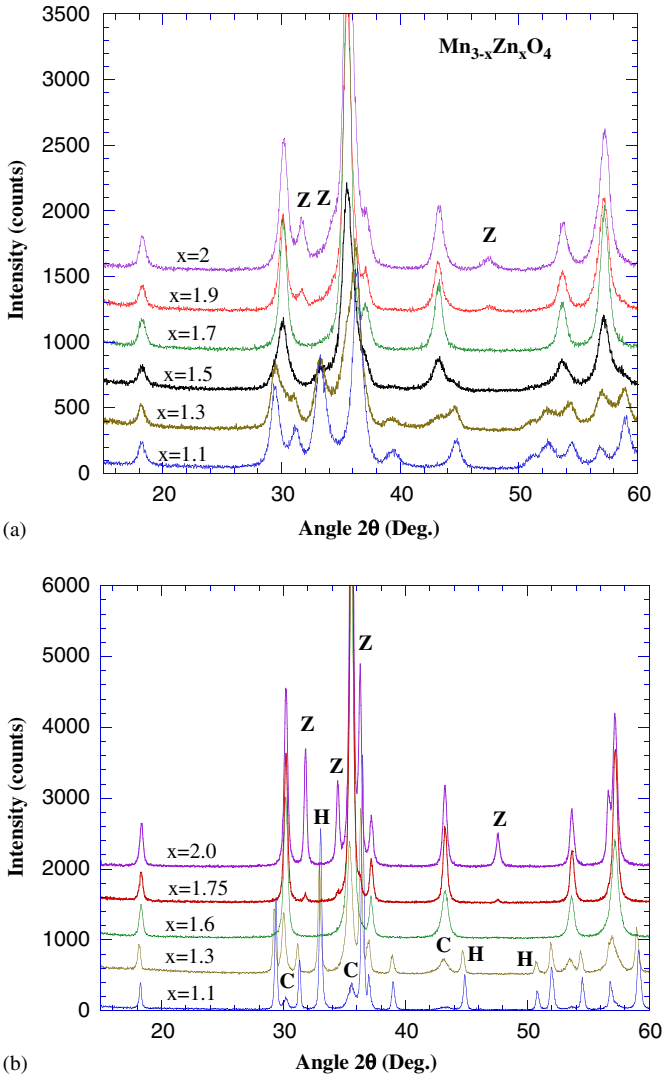

Fig. 1. (a) X-ray patterns of selected $Mn_{3-x}Zn_xO_4$ samples sintered at 450 °C for 16 h. (b) X-ray patterns of selected $Mn_{3-x}Zn_xO_4$ samples sintered at 600 °C for 16 h. The value of x is given for each pattern in the figures.

3. Results and discussion

Fig. 1a shows the X-ray patterns of selected $Mn_{3-x}Zn_xO_4$ samples sintered at 450 °C. They exhibit broad diffraction peaks owing to the low sintering temperature but the products are clearly formed. According to the patterns, four regions can be deduced for these compounds. The $x = 1$ sample (not shown here) exhibits peaks characteristics of the hetaerolite, $ZnMn_2O_4$ (H-phase). This compound is isostructural to the hausmannite, Mn_3O_4, and belongs to the spinel family with a tetragonal distortion owing to the presence of the active Jahn–Teller Mn^{3+} ion in the octahedral sites. Single phase pattern is observed for $x = 1.6$ (not shown) and $x = 1.7$. The X-ray patterns are typical of a cubic spinel (C-phase) whose space group is $Fd\bar{3}m$. Between both regions, $1.1 \leqslant x < 1.6$, the patterns show diffraction peaks of both phases and for

$x > 1.7$, the patterns reveal the presence of the cubic spinel and ZnO (denoted as *Z*-phase). The average crystal size for spinel phases was determined from X-ray patterns by using the Scherrer equation. It ranges between 120 and 150 Å for the whole series.

Fig. 1b shows the X-ray patterns for samples sintered at 600 °C for 16 h. The samples are now better crystallized but the phase distribution follows the same trend. The estimated crystal size is now between 700 and 850 Å for the spinel phases. Some samples ($x = 1.1$, 1.5, 1.7 and 1.9) were sintered for another 5 days and the only noticeable change was an increase of the crystallinity, the grain size being now well above 1000 Å. The X-ray patterns of samples sintered at 600 °C were used to quantify the proportions of phases present in each sample. Extrapolating the experimental data, we have found that the mixture of *C* and *H* phases exists between $x = 1.05$ and 1.55 whereas the mixture of *C* and *Z* phases appears at 1.72. Therefore, the stable region for *C* single phase at 600 °C ranges between $x = 1.55$ and $x = 1.72$. These limits are in agreement with our results for $Mn_{1.45}Zn_{1.55}O_4$ and $Mn_{1.25}Zn_{1.75}O_4$ compositions. Both samples exhibit tiny amounts of secondary phases at 600 °C (*H* and *Z*, respectively).

The *C*-phase also has a limited temperature range. The $x = 1.7$ and 1.6 samples heated at 700 °C and cooled in the furnace revealed broad diffraction peaks together to segregation of *Z*-phase. The thorough analysis of the patterns evidences the presence of two spinel phases, the *C*-phase and a new tetragonal spinel phase (hereafter denoted by *T*) with a smaller distortion with regard to *H*-phase. Both spinels show a poor crystallinity. In order to study the equilibrium state at 700 °C, some samples were quenched into water and the results can be seen in Fig. 2. The samples with $x \leqslant 1.5$ are composed by two tetragonal phases, *H* and *T*, whereas samples with $x > 1.55$ are formed

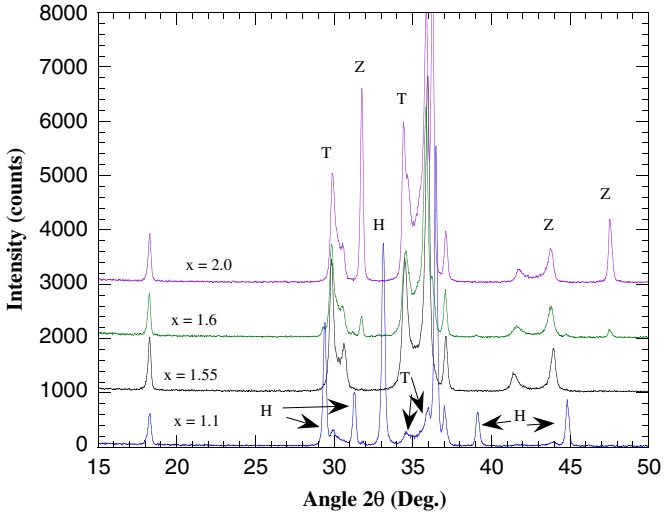

Fig. 2. X-ray patterns of selected $Mn_{3-x}Zn_xO_4$ samples sintered at 700 °C for 3*d* and quenched into room temperature. The value of *x* is given for each pattern.

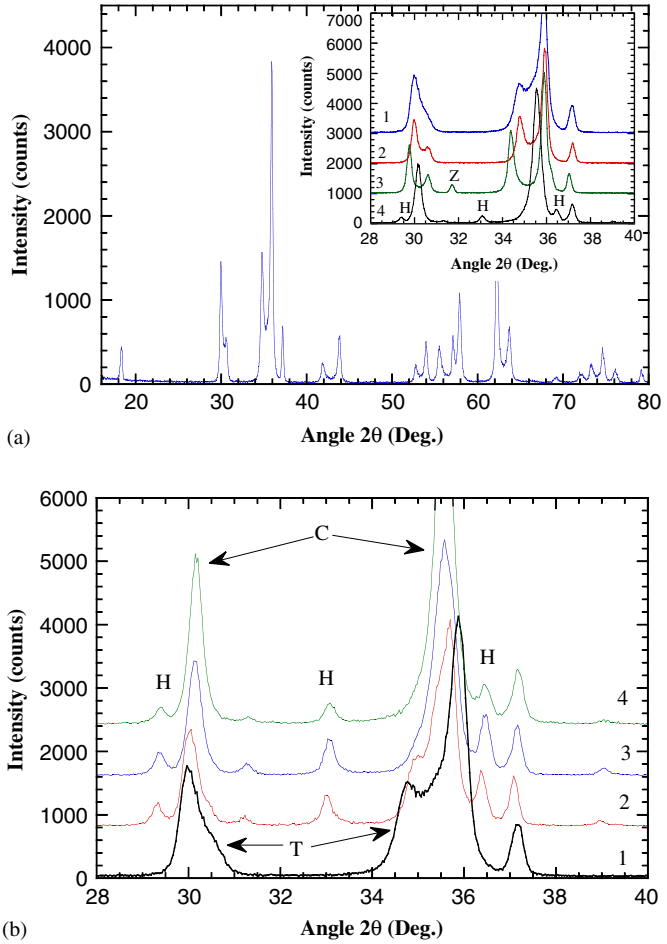

Fig. 3. (a) X-ray pattern for $Mn_{1.45}Zn_{1.55}O_4$ sintered at 700 °C for 3*d* and quenched into water. Inset: Comparison of X-ray pattern from $Mn_{1.45}Zn_{1.55}O_4$ samples sintered and cooled under different conditions. 1 refers to samples sintered at 700 °C and cooled in the furnace (300 °C h^{-1}). 2 is a sample sintered at 700 °C and quenched into water. 3 is a sample sintered at 800 °C and quenched into water. 4 is the sample sintered at 600 °C and cooled in the furnace. (b) Comparison of different $Mn_{1.45}Zn_{1.55}O_4$ samples. 1 stands for the sample sintered at 700 °C and cooled in the furnace. 2 is a quenched sample from 700 °C and annealed at 600 °C for 1*d*. 3 is the same sample as 2 after annealing for 3*d*. 4 stands for the sample obtained from direct sintering at 600 °C of the precursor.

by *T*- and *Z*-phases. Only the pattern of $Mn_{1.45}Zn_{1.55}O_4$ seems to be a single phase at a first glance (see also Fig. 3). Moreover, the presence of a single-phase for this composition agrees with the phase quantification of the *X*-ray patterns for the rest of the samples. However, the analysis of $Mn_{1.45}Zn_{1.55}O_4$ pattern reveals that in all cases, the *T* phase is accompanied by a parasitic *C*-phase. The presence of this phase could be understood in terms of kinetic arguments. In order to test it, $Mn_{1.45}Zn_{1.55}O_4$ was subject to different thermal treatments and the results are displayed in the inset of Fig. 3a. When the sample is cooled in the furnace (~5 °C/min), a significant amount of C-phase is present in the X-ray pattern. The amount of *C*-phase is strongly reduced in quenched samples but it does not disappear completely indicating that either *C*-phase is in its upper limit of stability or the transformation kinetics

is very fast for this transition on cooling. In any case, the *C*-phase undergoes a phase transition between 600° and 700 °C and the new stability region for a spinel single phase is located at $x \sim 1.55$.

The *T*-phase also has a limited temperature range. Samples quenched from 800 °C (see curve 3 in the inset of Fig. 3a) proved to have *Z*-phase together with a *T*-phase showing a higher tetragonal distortion. One can infer that stability region for single spinel phase shifts to lower values of x with increasing temperature. This shift is also inferred from the previous phase diagram reported in Ref. [12].

At this point, reasonably doubts can arise about the presence of two phases in $Mn_{1.45}Zn_{1.55}O_4$ at 600 °C. One can argue slow diffusion rates to justify the presence of the minor *H*-phase at the given temperature. In order to verify it, samples quenched from 700 °C (without *H*-phase) were annealed at 600 °C. The results are collected in Fig. 3b. Transformation from *T* to *C*-phase is clearly seen in the sample heated during 1*d* though the process did not end after 3*d* of annealing owing to the low diffusion rate. This transition is coupled to a segregation of *H*-phase as occurs by direct synthesis at 600 °C during more than 5*d*. This result makes evident that $Mn_{1.45}Zn_{1.55}O_4$ composition is biphasic at 600 °C.

Therefore, we can propose the tentative binary phase diagram indicated in Fig. 4. This diagram concurs with that reported in Ref. [12] at temperatures above 700 °C and completes the low-temperature region. In such a reference a *C*-phase is inferred but not experimentally isolated. However, two different tetragonally distorted spinels are clearly seen. In this work, we have demonstrated that *C*-phase is stable only at low temperature and in a narrow composition range. At temperatures above 700 °C, the spinels are all tetragonally distorted as indicated in Ref. [12].

This phase diagram also concurs with the Gibbs rule. If a system in thermodynamic equilibrium contains *P* phases and *C* components, then the Gibbs phase rule states that the number of degrees of freedom is given by $F = C - P + 2$.

In the case of Zn–Mn–O system, this rule connects the number of components ($C = 3$), the number of phases in equilibrium and the number of intensive variables (temperature and pressure). Therefore, the Gibbs rule predicts three coexisting phases at most. In practice, during the solid state reaction the oxygen content of the samples equilibrates with the oxygen partial pressure (pO_2) of the gas at the given temperature. Therefore, the oxygen content can be chosen freely by changing pO_2 of the gas phases and thus, there are three intensive variables (temperature, pressure and pO_2). Accordingly, two thermodynamic phases coexisting in equilibrium are expected and the phase relations of the Zn–Mn–O system can be visualized as a pseudo-binary phase diagram. In such a case, the x-axis is the cationic composition whereas the y-axis is the temperature (or pO_2 on varying the synthesis atmosphere). Such a phase diagram is displayed in Fig. 4. As expected, a maximum of two coexisting phases are observed except for a special case, the two-phase regions with T^* (in fact $T+C$). In this case, three phases may coexist if the temperature is near the upper or lower stability limit of one of the phases [15] though the presence of the *C*-phase may also be due to the kinetic reasons as mentioned above.

Therefore, this survey puts forward the presence of new cubic spinels in a narrow composition range of the Zn–Mn–O system. In order to characterize these samples, profile analysis has been performed for both samples using the Rietveld method. The results for $Mn_{1.3}Zn_{1.7}O_4$ sample is shown in Fig. 5 and the best fit parameters are summarized in Table 1. The fits are good supporting the existence of the cubic spinels. The lattice parameters and allowed reflections nicely square with the ones reported for $ZnMnO_3$ [10] suggesting that these authors obtained, in fact, this kind of cubic spinel. These are normal spinels whose tetrahedral sites are mainly occupied by Zn^{2+} ions. The best refinement was achieved for a small percentage of

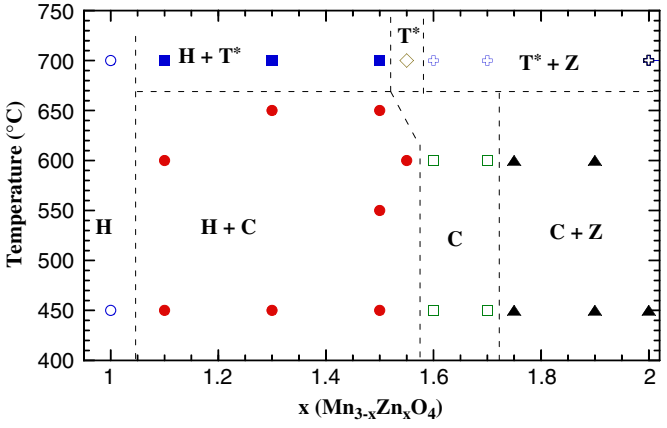

Fig. 4. Proposed phase diagram for part of the Zn–Mn–O system in air up to 700 °C. *H*, *Z*, *C* and *T* stands for hetaerolite, zincite, cubic spinel and tetragonal spinel phases, respectively. *T** indicates that secondary *C*-phase is also present and the exact amount depends on the cooling process.

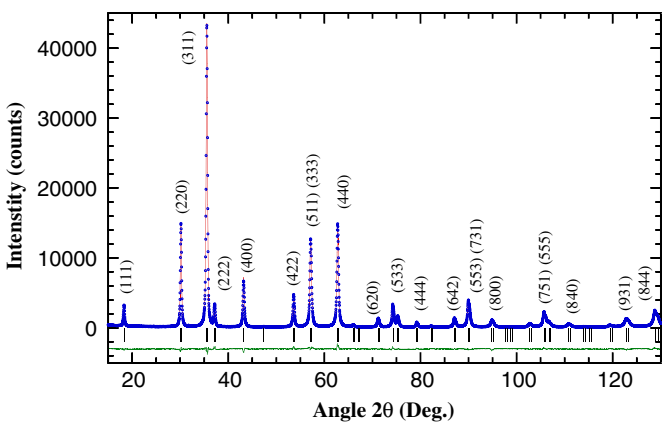

Fig. 5. X-ray refinement for $Mn_{1.3}Zn_{1.7}O_4$ sintered at 600 °C during 15 h. Points and line show experimental and fit data. The difference between both set of data is plotted at the bottom, below the tick marks of the allowed reflections.

Table 1
Refined lattice parameter, unit cell volume, structural parameters (site composition, temperature factors and fractional atomic coordinate), selected distances and reliability factors for $Mn_{1.4}Zn_{1.6}O_4$ and $Mn_{1.3}Zn_{1.7}O_4$ sintered at 600 °C

Sample	$Mn_{1.3}Zn_{1.7}O_4$	$Mn_{1.4}Zn_{1.6}O_4$
a (Å)	8.3676(1)	8.3646(4)
Volume (Å^3)	585.88(1)	585.24(5)
M_{tet} at (1/8 1/8 1/8):	$0.9Zn^{2+}$, $0.1Mn^{3+}$	$0.9Zn^{2+}$, $0.1Mn^{3+}$
B (Å^2)	0.24(1)	0.16(2)
M_{oct} at (1/2 1/2 1/2):	$0.8Zn^{2+}$, $0.5Mn^{3+}$, $0.7Mn^{4+}$	$0.7Zn^{2+}$, $0.7Mn^{3+}$, $0.6Mn^{4+}$
B (Å^2)	0.25(1)	0.15(2)
O at (x x x): x	0.2591(1)	0.2582(2)
B (Å^2)	1.07(3)	0.95(5)
M_{tet}–O (Å)	1.943(1)	1.930(1)
M_{oct}–O (Å)	2.019(1)	2.025(1)
R_p/R_{wp} (%)	4.2/5.9	6.7/9.4
R_{Bragg} (%)	2.1	2.9

Reliability factors are defined in Ref. [11]. Numbers in parenthesis refer to standard deviation of the last significant digit.

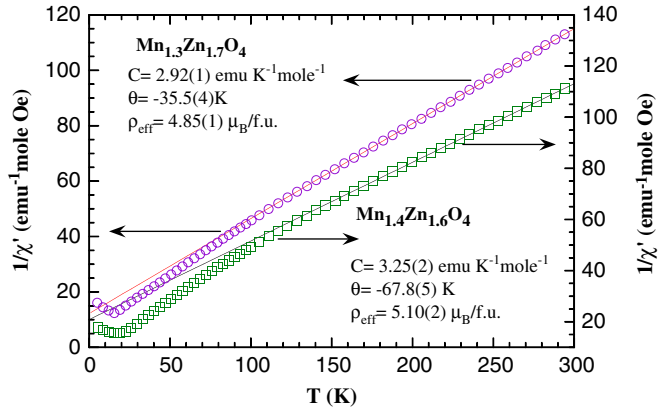

Fig. 6. Inverse of the AC magnetic susceptibility versus temperature for the samples are indicated in the plot. The straight lines are fits to the Curie–Weiss law.

inversion, namely $10\pm2\%$ of Mn^{3+} in the tetrahedral sites. The octahedral sites are then occupied by a mixture of Mn^{3+}, Mn^{4+} and Zn^{2+} ions as indicated in Table 1. The concentration of Mn^{3+} in octahedral sites is below the critical value of 60% in agreement with the formation of a cubic structure [16]. The unit cell is larger for $Mn_{1.3}Zn_{1.7}O_4$ which is in agreement with a higher concentration of Zn^{2+}, bigger than Mn^{3+} [17]. Finally, the bond lengths are in accordance to the values expected from tabulated ionic radii [17].

Magnetic properties have been characterized for the two new cubic spinels. The inverse of the AC magnetic susceptibility (χ_{AC}) for $Mn_{1.4}Zn_{1.6}O_4$ and $Mn_{1.3}Zn_{1.7}O_4$ is shown in Fig. 6. The $1/\chi_{AC}$ vs. temperature curve is linear at high temperature for both samples indicating that the Curie–Weiss law is obeyed in a wide temperature range. Accordingly, we have fitted these data to the equation: $\chi = C/(T-\theta)$ where C and θ are the Curie and Weiss constants, respectively. C is related to the effective paramagnetic moment by means of the expression $C = N\mu_B^2\rho_{eff}^2/3K_B$, where N, μ_B, ρ_{eff} and K_B denote Avogadro number, Bohr magneton, effective paramagnetic moment and Boltzmann's constant, respectively. The best-fit parameters are also summarized in Fig. 6. The calculated paramagnetic moments are 5.10 and 4.85 μ_B/f.u. for $Mn_{1.4}Zn_{1.6}O_4$ and $Mn_{1.3}Zn_{1.7}O_4$, respectively. These values correlate quite well with the expected ones from the spin-only contribution of the formal mixture of Mn^{3+} and Mn^{4+} ions which are 5.25 and 4.95 μ_B/f.u. for $x = 1.6$ and 1.7, respectively. The negative value of θ suggests the presence of antiferromagnetic correlations in the paramagnetic region. These correlations increases as the Mn content increases in agreement with the diminution of the non-magnetic Zn^{2+} ions.

The magnetic susceptibility at low temperature reveals the presence of peaks at ~19 and at ~15 K for $Mn_{1.4}Zn_{1.6}O_4$ and $Mn_{1.3}Zn_{1.7}O_4$, respectively. In order to gain insight into the origin of these anomalies, DC magnetization and AC measurements at several frequencies have been carried out. The results are displayed in Fig. 7 for $Mn_{1.3}Zn_{1.7}O_4$. The ZFC curve exhibit a peak in accordance to the AC measurement. Such peak is lacked in the FC branch where the magnetization keeps on increasing below 15 K. In fact, the divergence between FC and ZFC curves begin at the peak temperature and this feature is typical of a spin-glass [18]. In this way, a dynamic behavior is clearly observed in the AC magnetic measurements displayed in the inset of Fig. 7. The height of the peak slightly decreases and it is shifted to higher temperatures with increasing the frequency of the AC field. This dynamic behavior is also characteristic of a spin-glass system. The frequency (ν) shift of the peak temperature (T_f) is usually characterized by the term $\Delta T_f/(T_f \Delta \ln \nu)$. In both samples, this term values around 8.5×10^{-3} which is in agreement with tabulated spin-glasses [18,19].

Therefore, the magnetic measurements confirm the presence of a spin-glass-like phase for both samples. This implies the presence of competitive interactions and randomness leading to magnetic frustration [19]. Randomness is very likely to arise from the presence of non-magnetic Zn^{2+} ions in both, octahedral and tetrahedral sites (see Table 1). Nevertheless, it is not obvious which interactions are in competition for an AB_2O_4 spinel. Normally, the A–B interaction is dominant and a collinear ferrimagnetic ground state is favored. In the present compounds, however, the tetrahedral sites are mainly occupied by non-magnetic Zn^{2+} ion which is very likely to weaken the A–B interaction. Therefore, the B–B interaction competes and even it could overcome the A–B one. Looking at the octahedral B-sites, they are occupied by Mn^{3+}, Mn^{4+} and Zn^{2+} ions if we consider an ionic approximation. The two magnetic ions have different electronic configurations in an octahedral environment,

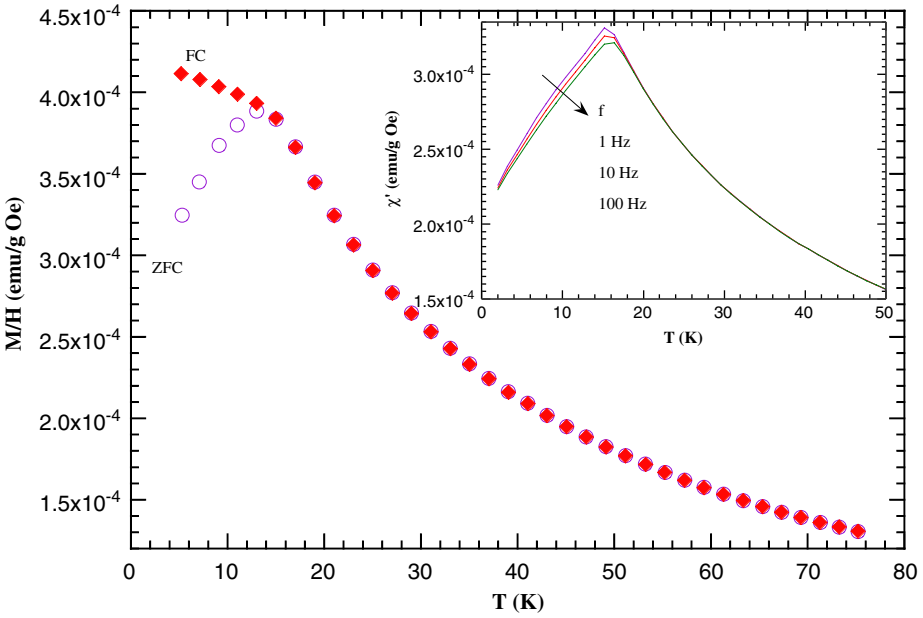

Fig. 7. Magnetization versus temperature for $Mn_{1.3}Zn_{1.7}O_4$ using an external field of 1 kOe. ZFC and FC stand for zero field cooling and field cooling, respectively. Inset: AC magnetic susceptibility vs. temperature for the same sample at different frequencies of the AC magnetic field. The arrow indicates the way of increasing frequency.

namely $t_{2g}^3e_g^1$ and $t_{2g}^3e_g^0$ for Mn^{3+} and Mn^{4+} ions, respectively. Since octahedra are sharing edges, the expected main magnetic interaction is a superexchange coupling with a 90° configuration and two bridging oxygens. The Goodenough–Kanamori rules [20] predict ferromagnetic interactions for $t_{2g}^3e_g^0 - O - t_{2g}^3e_g^0$ and $t_{2g}^3e_g^1 - O - t_{2g}^3e_g^1$ configurations whereas antiferromagnetic interaction is inferred for the $t_{2g}^3e_g^0 - O - t_{2g}^3e_g^1$ configuration. These competitive interactions together to the structural disorder produced by non-magnetic Zn^{2+} ions is expected to cause the spin-glass ground state observed in our magnetic measurements.

4. Conclusions

The low temperature phase diagram of Zn–Mn–O system in air has been studied. High reactive precursors were used to increase the diffusion rates and in practice, final compounds can be formed by sintering at 450 °C during 16 h. This study demonstrates the existence of cubic spinels in this system. They are stable at low temperature (~600 °C) and in a narrow composition range (x~1.6–1.7). They are normal spinels with a small degree of inversion (around 10%). Upon heating, they undergo a structural phase transition giving rise to a tetragonal spinel. This spinel shows a small distortion with regard to hausmannite or hetaerolite phases. At 700 °C, the single phase region is reduced and shifted to lower values of x (~1.55).

Magnetic properties have been characterized for the cubic spinels. They obey a Curie–Weiss law in a broad temperature range in agreement with the presence of the theoretical mixture of Mn^{3+} and Mn^{4+} ions. Magnetic anomalies at very low temperature reveal the presence of competitive magnetic interactions giving rise to the developing of a spin-glass phase. The dynamic behavior of this phase is in accordance to the reported one for canonical spin-glasses.

Acknowledgments

Financial support from CICyT and DGA (projects MAT2005-04562 and PIP018/2005) are acknowledged. We also thank M.C. Sánchez and the Servicio Nacional EXAFS of Zaragoza University from technical support in the acquisition of X-ray patterns.

References

[1] K. Sato, H. Katayama-Yoshida, Jpn. J. Appl. Phys. 40 (2001) L334; K. Sato, H. Katayama-Yoshida, Physica B 308–310 (2001) 904.
[2] R. Janisch, P. Gopal, N.A. Spaldin, J. Phys.: Condens. Matter 17 (2005) R657.
[3] P. Sharma, A. Gupta, K.V. Rao, F.J. Owens, R. Sharma, R. Ahuja, J.M.O. Guillen, B. Johansson, G.A. Gehring, Nat. Mater. 2 (2004) 673;
P. Sharma, A. Gupta, F.J. Owens, A. Inoue, K.V. Rao, J. Magn. Magn. Mater. 282 (2004) 115.
[4] S. Kolesnik, B. Dabrowski, J. Appl. Phys. 96 (2004) 5379;
S. Kolesnik, B. Dabrowski, J. Mais, J. Appl. Phys. 95 (2004) 2582.
[5] D.C. Kundaliya, S.B. Ogale, S.E. Lofland, S. Dhars, C.J. Metting, S.R. Shinde, Z. Ma, B. Varughese, K.V. Ramanujachary, L. Salamanca-Riba, T. Venkatesan, Nat. Mater. 3 (2004) 709.
[6] M.A. García, M.L. Ruiz-González, A. Quesada, J.L. Costa-Kramer, J.F. Fernández, S.J. Khatib, A. Wennberq, A.C. Caballero, M.S. Martín-González, M. Villegas, F. Briones, J.M. González-Calbet, A. Hernando, Phys. Rev. Lett. 94 (2005) 217206.

[7] J. Blasco, F. Bartolomé, L.M.García, J. García, J. Mater. Chem. (2006), doi:10.1039/b518418e.
[8] S. Kolesnik, B. Dabrowski, J. Mais, J. Supercond. 15 (2002) 251.
[9] K. Izumiya, E. Akiyama, H. Habazaki, A. Kawashima, K. Asami, K. Hashimoto, N. Kumagai, J. Appl. Electrochem. 27 (1997) 1362.
[10] H. Toussaint, Rev. Chim. Min. 1 (1964) 141.
[11] B.L. Chamberland, A.W. Sleight, J.F. Weiher, J. Sol. State Chem. 1 (1970) 512.
[12] F.C.M. Driessens, G.D. Rieck, J. Inorg. Nucl. Chem. 28 (1966) 1593.
[13] J. Blasco, M. Castro, J. García, J. Phys.: Condens. Matter 6 (1994) 5875.
[14] J. Rodríguez-Carvajal, Physica B 192 (1992) 55 Available at www-llb.cea.fr.
[15] J.M. Paulsen, J.R. Dahn, Chem. Mater. 11 (1999) 3065.
[16] A. Navrotsky, O.J. Kleppa, J. Inorg. Nucl. Chem. 29 (1967) 2701.
[17] R.D. Shannon, Acta Crystallogr. A 32 (1976) 751.
[18] J. Blasco, J. García, G. Subías, M.C. Sánchez, Phys. Rev. B 70 (2004) 094426.
[19] J.A. Mydosh, Spin Glasses, An Experimental Introduction, Taylor & Francis, London, 1993.
[20] J. Kanamori, J. Phys. Chem. Solids 10 (1959) 87;
M. Atanasov, S. Angelov, Chem. Phys. 150 (1991) 383.